All-fiber ring Raman laser generating parabolic pulses

V. I. Kruglov, D. Méchin,* and J. D. Harvey
Physics Department, The University of Auckland, Private Bag 92019, Auckland, New Zealand
(Received 23 July 2009; published 16 February 2010)

We present theoretical and numerical results for an all-fiber laser using self-similar parabolic pulses ("similaritons") designed to operate using self-similar propagation regimes. The similariton laser features a frequency filter and a Sagnac loop which operate together to generate an integrated all-fiber mode-locked laser. Numerical studies show that this laser generates parabolic pulses with linear chirp in good agreement with analytical predictions. The period for propagating similariton pulses in stable regimes can vary from one to two round trips for different laser parameters. Two-round-trip-period operation in the mode-locked laser appears at bifurcation points for certain cavity parameters. The stability of the similariton regimes has been confirmed by numerical simulations for large numbers of round trips.

DOI: 10.1103/PhysRevA.81.023815 PACS number(s): 42.60.Fc, 42.65.Jx, 42.81.Dp, 42.25.Fx

I. INTRODUCTION

Pulse formation in modern femtosecond lasers is generally mediated by the interplay between dispersion and nonlinearity. In these cases, a self-focusing nonlinearity is balanced by anomalous group velocity dispersion (GVD) [1,2]. Such lasers have segments of normal and anomalous GVD and the net or path-averaged cavity dispersion can be normal, zero, or anomalous. In the cases when the net GVD approaches zero, stretched-pulses can occur [3], described by breathing solutions. Such fiber lasers can have pulse energies an order of magnitude higher than soliton lasers. More complex pulse formation and pulse evolution occurs when the cavity GVD approaches zero and finally becomes normal. It has been demonstrated [4] that the resulting lengthy pulses are highly chirped, in agreement with the theory [2]. Pulse shaping in such a laser is based on spectral filtering of the chirped pulse, which cuts off the temporal wings of the pulse. Mode-locked laser operation with large net normal GVD is expected to lead to stable high-energy pulses [5].

Self-similar parabolic pulses ("similaritons") with a linear chirp generated in optical-fiber amplifiers with normal GVD have generated considerable interest in recent years. Asymptotically exact similaritons have been found and experimentally observed for propagation in optical-fiber amplifiers [6–9]. The results of these theoretical, experimental and numerical studies have recently found increasing practical application in high-power amplifier systems, efficient temporal compressors [10–16], and similariton lasers. The similariton solution also has been found in the growth of trapped Bose-Einstein condensates (BECs) [17] and for trapped BECs in $3+1$ dimensions [18]. Recently, the self-similar laser [19] and so-called chirped-pulse oscillator (CPO) [20] have been investigated for large net normal GVD to achieve higher pulse energies [21,22]. Both self-similar and CPO lasers generate high pulse energies with femtosecond dechirped pulse durations [23–25]. The pulses propagating in self-similar lasers are parabolic and highly chirped.

The stability of the pulse generation from one round trip to another in a laser is an important quantity for applications in optics and telecommunications [26–28]. Pulse evolution with periodic changes of the pulse energy from one round trip to another can also yield stable [29] and useful devices. The impact of amplified spontaneous emission noise and Raman-induced imperfections in amplification where calculated for optical-fiber communication systems in Refs. [30–32].

We report here theoretical and numerical predictions for the generation of parabolic pulses in an all-fiber ring laser with Raman amplification. These similariton pulses tend toward a parabolic shape and accumulate a linear chirp, in agreement with theoretical predictions. We have observed that the frequency filter and Sagnac loop operating as one integrated unit can yield mode-locked laser operation for this similariton laser. The all-fiber similariton laser presented here (Fig. 1), supported by a full analytical model, is designed to operate using self-similar propagation regimes. For appropriate laser parameters, it demonstrates stable operating regimes with period-one and period-two round-trip operation. We call such stable regimes similariton period-one (SP1) and similariton period-two (SP2). The new period-two operation in the mode-locked laser regime appears at bifurcation points for certain lengths of the second compression segment of the cavity. We have confirmed the stability of the similariton regimes by direct numerical simulations for large numbers of round trips.

II. DESIGN AND THEORY OF A SIMILARITON LASER WITH RAMAN GAIN

The schematic diagram of the laser is shown in Fig. 1. The operating wavelength of the laser has been chosen to be close to 1535 nm so that a pump at a wavelength close to 1445 nm can be used. The pump is launched and extracted from the cavity using wavelength division multiplexor (WDM) couplers. A backward pumping scheme is used to avoid pump depletion and linear loss is neglected in the gain fiber, so g_s is considered constant along the similariton stage. The first stage where the similariton propagation takes place is constructed using a dispersion-compensating fiber (DCF) in order to have positive GVD around 1535 nm. The length of the fiber has been chosen to be long enough to generate a parabolic pulse; that is, the asymptotic regime is reached at point A. Then

*Present address: PERFOS, 11 Rue de Broglie, 22300 Lannion, France.

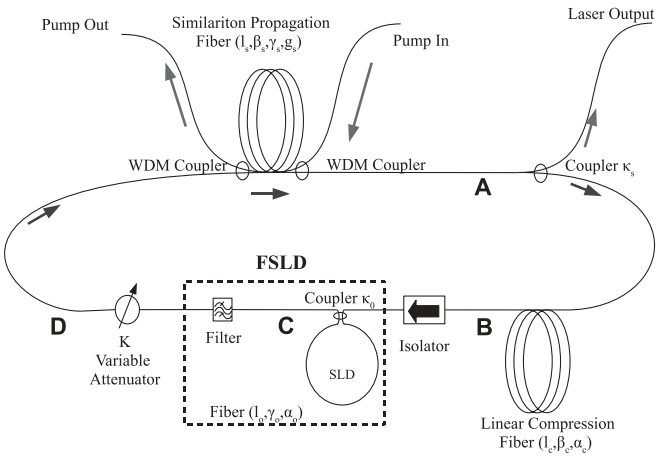

FIG. 1. Schematic diagram of the similariton ring laser.

a coupler is used to extract most of the light in the laser output. The parabolic chirped pulse is then linearly compressed at point B using a suitable anomalous dispersion regime fiber. A Sagnac loop device (SLD) made of highly nonlinear fiber and an asymmetric coupler is then used to initiate and stabilize the mode locking and is preceded by an isolator which ensures unidirectional operation while removing unwanted backreflection from the SLD. The phenomenon of self-phase modulation (SPM) has resulted in the use of highly nonlinear fiber for the SLD. At point C a frequency filter reshapes the spectrum of the pulse and removes most of the the SPM-induced chirp due to the SLD and a variable attenuator is finally used to set the right energy before the initial stage (at point D).

A. Similariton propagation segment

The theoretical description of pulse shaping and propagation in the all-fiber ring similariton laser with Raman pump and amplification within first section s (similariton propagation segment) is based on the generalized nonlinear Schrödinger equation (GNLSE) with bandwidth-limited gain [33]:

$$i\frac{\partial\psi_s}{\partial z}=\frac{\beta_s}{2}\frac{\partial^2\psi_s}{\partial\tau^2}-\gamma_s|\psi_s|^2\psi_s+i\frac{g_s}{2}\psi_s+i\frac{\sigma g}{2}\frac{\partial^2\psi_s}{\partial\tau^2}. \quad (1)$$

Here $\psi_s(z,\tau)$ is the complex envelope of the electrical field in a comoving frame; τ is the retarded time; β_s is the normal GVD parameter; γ_s is the nonlinearity parameter; $g_s=g-\alpha_s$ is the the effective Raman gain parameter, where α_s is the loss parameter; and $\sigma=1/\Omega_g^2$ is the parameter of the bandwidth-limited gain in the fiber. However, our simulations show that for parabolic (similariton) regimes of the laser the last term in Eq. (1) is very small compared with the amplification term and hence can be neglected. We design the laser parameters and particularly choose the length l_s of the first propagation section for given parameters β_s, γ_s, and g_s so that the pulse shape at the distance $z=l_s$ will be close to the asymptotic parabolic solution [6–8]:

$$\psi_s(\tau)=A_s\sqrt{1-\left(\frac{\tau}{\tau_s}\right)^2}\exp[i\Phi_s(\tau)]\theta(\tau_s-|\tau|), \quad (2)$$

where $\psi_s(\tau)\equiv\psi_s(l_s,\tau)$ and $\theta(\tau)$ is the Heaviside step function. The amplitude A_s and the width τ_s of the similariton pulse are

$$A_s=\frac{1}{2}\left(\frac{2g_s^2E_0^2}{\beta_s\gamma_s}\right)^{1/6}\exp\left(\frac{1}{3}g_sl_s\right), \quad (3)$$

$$\tau_s=3\left(\frac{\beta_s\gamma_sE_0}{2g_s^2}\right)^{1/3}\exp\left(\frac{1}{3}g_sl_s\right). \quad (4)$$

The phase $\Phi_s(\tau)$ of the parabolic pulse and the energy E_0 of the input pulse at $z=0$ are given by

$$\Phi_s(\tau)=\Phi_0+\frac{3\gamma_s}{2g_s}A_s^2-\frac{g_s}{6\beta_s}\tau^2, \quad (5)$$

$$E_0=\int_{-\infty}^{+\infty}|\psi_0(\tau)|^2d\tau, \quad (6)$$

with $\psi_0(\tau)\equiv\psi_s(0,\tau)$. The energy E_s of the parabolic pulse for the propagating length l_s is $E_s=E_0e^{g_sl_s}$. Clearly, the asymptotical parabolic pulse (Fig. 5) has a linear chirp $\Omega_s(\tau)=g_s\tau/(3\beta_s)$ which is an important condition for pulse compression in the compression segment of the ring similariton laser (Fig. 7). Most of the pulse energy is extracted at this point A by the output coupler.

B. Compression segment

In the second compression segment, the energy of the pulse has been greatly reduced by the output coupler and we assume linear compression in this segment. If necessary, this segment could be implemented using a suitable hollow core fiber to minimize nonlinear effects. If we designate κ_s as the similariton output couple parameter (see Fig. 1) and l_c as the length of the second compression segment, then the function $\psi_c(z,\tau)$ in the end of a second segment is

$$\psi_c(l_c,\tau)=\sqrt{\kappa_s}\int_{-\infty}^{+\infty}\mathcal{G}(l_c,\tau-\tau')\psi_s(\tau')d\tau'. \quad (7)$$

Here $\mathcal{G}(l_c,\tau-\tau')$ is the Green function of the linear Schrödinger equation for propagation distance $z=l_c$ with anomalous GVD and the absorption coefficient equal to β_c and α_c, respectively:

$$\mathcal{G}(l_c,\tau-\tau')=\sqrt{\frac{i}{2\pi\beta_cl_c}}\exp\left[-\frac{\alpha_cl_c}{2}-\frac{i(\tau-\tau')^2}{2\beta_cl_c}\right]. \quad (8)$$

In the case when the GVD in the second compression segment is distance dependent $\beta_c=\beta_c(z)$, one should replace β_c with the average value $\bar{\beta}_c$ in Eq. (8), where $\bar{\beta}_c=l_c^{-1}\int_0^{l_c}\beta_c(z)dz$.

In the second segment l_c is chosen so that the pulse is unchirped as it enters the similariton segment [i.e., $\psi_0(\tau)=\psi_s(0,\tau)$ is unchirped]. This condition provides a minimal level of noise around the similariton pulse, which is important for the stability of the mode-locked pulse regimes. Otherwise, the noise in the wings of the pulse grows after each round trip and, as a result, mode locking cannot be achieved. The chirp of the pulse at the end of the second segment (at $z=l_c$) for $\tau=0$ should also be close to zero. This requirement has been obtained by exploring extensive numerous numerical simulations, and it has been found to be important for optimization of the laser parameters in stable regimes. In the Appendix it is shown that in the vicinity

of the length $z = \tilde{l}_c$, where the chirp of the pulse is zero, the function $\psi_c(z, \tau)$, with good accuracy, is the Gaussian function (Fig. 5)

$$\psi_c(z,\tau) = \frac{4}{3}\sqrt{\frac{2\kappa_s}{\pi}}(1+G^2)^{1/4}A_s \times \exp\left[-\frac{\alpha_c z}{2} - \frac{\tau^2}{2\tau_c^2} - \frac{i}{2}\mathcal{C}(z)\tau^2\right]e^{i\Phi_c}, \quad (9)$$

where the phase is given by

$$\Phi_c = a + \frac{1}{2}\arctan(-G), \quad a = \Phi_0 + \frac{3\gamma_s A_s^2}{2g_s}. \quad (10)$$

The function $\mathcal{C}(z)$ characterizing the chirp of the pulse $\Omega_c(z, \tau) = \mathcal{C}(z)\tau$ has the form

$$\mathcal{C}(z) = \frac{G}{\tau_c^2} - \frac{|\beta_c|}{\tau_c^4}z, \quad (11)$$

with

$$G = \frac{3\pi g_s \tau_s^2}{64\beta_s}. \quad (12)$$

The characteristic width τ_c of the pulse and the characteristic length $\tilde{l}_c$ defined by the equation $\Omega_c(\tilde{l}_c, \tau) = 0$ are

$$\tau_c = \frac{3\sqrt{\pi}\tau_s}{8\sqrt{1+G^2}}. \quad (13)$$

$$\tilde{l}_c = \frac{G\tau_c^2}{|\beta_c|}. \quad (14)$$

For the parameters of the laser (see Sec. V), we find that $G \gg 1$ ($G \simeq 270$). In this case, the preceding equations can be simplified by changing $1 + G^2$ to G^2. Using Eqs. (3) and (4), we may present the Gaussian function $\psi_c(z, \tau)$ as

$$\psi_c(z,\tau) = \left(\frac{\kappa_s E_0}{\sqrt{\pi}\tau_c}\right)^{1/2} \exp\left[\frac{g_s l_s}{2} - \frac{\alpha_c z}{2} - \frac{\tau^2}{2\tau_c^2} - \frac{i}{2}\mathcal{C}(z)\tau^2\right] \times e^{i(a-\pi/4)}, \quad (15)$$

where the phase function $\mathcal{C}(z)$ is

$$\mathcal{C}(z) = \frac{G}{\tau_c^2}\left(1 - \frac{z}{\tilde{l}_c}\right) = \frac{|\beta_c|(\tilde{l}_c - z)}{\tau_c^4}. \quad (16)$$

Here the width τ_c of the pulse and the length $\tilde{l}_c$ are

$$\tau_c = \frac{8\beta_s}{\sqrt{\pi}g_s\tau_s}, \quad (17)$$

$$\tilde{l}_c = \frac{3\beta_s}{g_s|\beta_c|}. \quad (18)$$

If $\beta_c = \beta_c(z)$ is distance dependent the approximate equation for length $\tilde{l}_c$ is given by $3\beta_s/g_s \simeq \int_0^{\tilde{l}_c} |\beta_c(z)|dz$. The energy of the pulse describing by the wave function $\psi_c(z, \tau)$ in Eq. (15) is

$$E_c(E_0, l_c) = \int_{-\infty}^{+\infty} |\psi_c(l_c, \tau)|^2 d\tau = \kappa_s E_0 \exp(g_s l_s - \alpha_c l_c). \quad (19)$$

We emphasize that the energy E_c found in Eq. (19) is exact. In this section we neglect the nonlinear effects using a suitable hollow core fiber. This means that the condition $L_D/L_{NL} \ll 1$ should be fulfilled in the compression segment where L_D is the dispersion length and L_{NL} is the nonlinear length. This condition written in an explicit form is

$$\kappa_s \gamma_c l_c A_s^2 e^{-\alpha_c l_c} \ll 1. \quad (20)$$

All the preceding equations are in a good agreement with numerical simulations when the distance $z = l_c$ is close to the characteristic length $\tilde{l}_c$: $|l_c - \tilde{l}_c|/\tilde{l}_c \ll 1$ (see Fig. 5). For example, the characteristic length $\tilde{l}_c$ given by Eq. (18) deviates from the exact result by about 1%.

C. Filter-Sagnac loop device

In the scheme presented here the feedback of the similariton laser is provided by integration of the Sagnac interferometer with a frequency filter. This integration is important for the mode-locking mechanism because in the stable similariton regimes the input pulse $\psi_0(\tau) = \psi_s(0, \tau)$ in the similariton segment s should be unchirped. Otherwise, the similariton pulses in segment s have small noise satellites, which are amplified for each round trip and destroy the stability of the mode-locking mechanism. We call such a nonlinear device an FSLD (filter-Sagnac loop device) because it operates as one integrated unit (see later in this article).

Assuming the nonlinearity-dominant regime ($L_D/L_{NL} \gg 1$) in the Sagnac loop, the output function $\psi_f(\tau)$ of the Sagnac loop is given by

$$\psi_f(\tau) = \{\kappa_0 \exp[i\kappa_0\gamma_0 L_0|\psi_c(l_c, \tau)|^2] - (1-\kappa_0) \times \exp[i(1-\kappa_0)\gamma_0 L_0|\psi_c(l_c, \tau)|^2]\}\psi_c(l_c, \tau), \quad (21)$$

where the effective length L_0 of the loop is $L_0 = [1 - \exp(-\alpha_0 l_0)]/\alpha_0$. Here κ_0 is the coupling parameter of the loop and γ_0 and α_0 are the nonlinear parameter and the absorption coefficient, respectively. To prevent amplification of the noise in each round trip, which destroys the stability of the mode-locking mechanism, we also use in our laser designs the switching condition [33] given by

$$L_0 = \frac{1 - \exp(-\alpha_0 l_0)}{\alpha_0} = \frac{\pi}{\gamma_0|1 - 2\kappa_0||\psi_c(l_c, 0)|^2}. \quad (22)$$

We note that the nonlinear feedback is considerable when the parameter κ_0 is close to 0.5 ($\kappa_0 \neq 0.5$). Thus, we also assume that the condition $|1 - 2\kappa_0| \ll 1$ is satisfied.

If we define $H(\omega)$ as the frequency filter function, then the output filter function $\psi_F(\tau)$ is given by

$$\psi_F(\tau) = \frac{1}{2\pi}\int_{-\infty}^{+\infty} H(\omega)\Psi_f(\omega)e^{-i\omega\tau}d\omega, \quad (23)$$

with $\Psi_f(\omega) = \int_{-\infty}^{+\infty} \psi_f(\tau)e^{i\omega\tau}d\tau$. Thus, Eqs. (21) and (23) yield the equation for the output filter fuction $\psi_F(\tau)$ as

$$\psi_F(\tau) = \kappa_0 \int_{-\infty}^{+\infty} h(\tau - \tau')\exp[i\kappa_0\gamma_0 L_0|\psi_c(l_c, \tau')|^2] \times \psi_c(l_c, \tau')d\tau' - (1-\kappa_0)\int_{-\infty}^{+\infty} h(\tau - \tau') \times \exp[i(1-\kappa_0)\gamma_0 L_0|\psi_c(l_c, \tau')|^2]\psi_c(l_c, \tau')d\tau'. \quad (24)$$

Here the filter function $h(\tau)$ is given by

$$h(\tau) = \frac{1}{2\pi}\int_{-\infty}^{+\infty} H(\omega)e^{-i\omega\tau}d\omega. \tag{25}$$

We assume later in this article that the characteristic filter width τ_h of the filter function $h(\tau)$ is much greater than the width τ_c of the output pulse in the second segment given by function $\psi_c(\tau)$: $\tau_h \gg \tau_c$. This is a necessary condition for this scheme of ring laser because it yields the mode-locking laser regimes. From Eq. (24) and condition $\tau_h \gg \tau_c$ follows that in this case the output pulse shape of the FSLD is completely defined by filter function $h(\tau)$:

$$\begin{aligned} \psi_F(\tau) &= R(E_0, l_c)h(\tau), \\ R(E_0, l_c) &= \kappa_0 R_1(E_0, l_c) - (1-\kappa_0)R_2(E_0, l_c), \end{aligned} \tag{26}$$

with the complex amplitudes $R_1(E_0, l_c)$ and $R_2(E_0, l_c)$ as

$$R_1(E_0, l_c) = \int_{-\infty}^{+\infty} \exp[i\kappa_0\gamma_0 L_0|\psi_c(l_c, \tau)|^2]\psi_c(l_c, \tau)d\tau, \tag{27}$$

$$R_2(E_0, l_c) = \int_{-\infty}^{+\infty} \exp[i(1-\kappa_0)\gamma_0 L_0|\psi_c(l_c, \tau)|^2]\psi_c(l_c, \tau)d\tau. \tag{28}$$

Thus, Eq. (26) shows that the FSLD operates as one unit: the shape of the output pulse $\psi_F(\tau)$ of the FSLD is given by the filter function $h(\tau)$, but the amplitude $R(E_0, l_c)$ is defined by the parameters of the Sagnac loop and the function $\psi_c(l_c, \tau)$, which depends on the energy E_0.

D. Threshold condition

From the periodic boundary condition for the propagating pulse it also follows that the input field in the first segment is $\psi_s(0, \tau) = K^{1/2}\psi_F(\tau) = K^{1/2}R(E_0, l_c)h(\tau)$, where $K \leqslant 1$ is the parameter of the variable attenuator, which is located after the FSLD. This allows us to find the energy [Eq. (6)] of the input pulse in the first segment by the following equation:

$$\begin{aligned} E_0 &= K|R(E_0, l_c)|^2 \int_{-\infty}^{+\infty} |h(\tau)|^2 d\tau \\ &= K|R(E_0, l_c)|^2 \frac{1}{2\pi}\int_{-\infty}^{+\infty} |H(\omega)|^2 d\omega. \end{aligned} \tag{29}$$

Let us introduce the function $Q(E_0, l_c)$, which defines the loss of the energy in the FSLD:

$$Q(E_0, l_c) = \frac{|R(E_0, l_c)|^2}{2\pi E_c(E_0, l_c)}\int_{-\infty}^{+\infty} |H(\omega)|^2 d\omega. \tag{30}$$

Then using Eq. (29) we find the relation $E_0 = KQ(E_0, l_c)E_c(E_0, l_c)$, with $E_c(E_0, l_c) = \kappa_s E_0 \exp(g_s l_s - \alpha_c l_c)$. Now, taking into account this expression for energy E_c and equation $E_0 = KQE_c$, we find the laser threshold condition:

$$KQ(E_0, l_c)\kappa_s \exp(g_s l_s - \alpha_c l_c) = 1. \tag{31}$$

Note that in the case where the laser exhibits additional loss in junctions, one should just redefine the parameters α_s, α_c, α_0, and κ_s, in the preceding equations.

If we consider, for example, the case when the filter function $H(\omega)$ is Gaussian $H(\omega) = \exp(-\tau_h^2\omega^2/2)$, where τ_h is the filter width, then the function $h(\tau)$ is

$$h(\tau) = \frac{1}{2\pi}\int_{-\infty}^{+\infty} H(\omega)e^{-i\omega\tau}d\omega = \frac{1}{\sqrt{2\pi}\tau_h}\exp\left(-\frac{\tau^2}{2\tau_h^2}\right). \tag{32}$$

Because we assume here that the condition $\tau_h \gg \tau_c$ is satisfied, the input pulse function in the first segment is $\psi_0(\tau) = K^{1/2}\psi_F(\tau)$, where the function $\psi_F(\tau)$ is defined by Eq. (26). Hence, in this case the input pulse function has the Gaussian shape (see Fig. 5),

$$\psi_0(\tau) = \left(\frac{E_0}{\sqrt{\pi}\tau_h}\right)^{1/2}\exp\left(-\frac{\tau^2}{2\tau_h^2}\right)e^{i\Phi_0}, \tag{33}$$

and the input energy E_0 can be found using the following equation:

$$E_0 = \frac{K|R(E_0, l_c)|^2}{2\sqrt{\pi}\tau_h}. \tag{34}$$

The loss of the energy in the FSLD is given by Eq. (30), and hence, in the case of Gaussian filter function, the loss function $Q(E_0, l_c)$ in the laser threshold Eq. (31) has the form

$$Q(E_0, l_c) = \frac{|R(E_0, l_c)|^2}{2\sqrt{\pi}\tau_h E_c(E_0, l_c)}. \tag{35}$$

We emphasize that the laser threshold condition given by Eq. (31) is equivalent to Eq. (29). Thus, this condition also can be written in the form $E_0 = F(E_0, l_c)$, where $F(E_0, l_c)$ is the output energy after one round trip as a function of the input energy E_0 (see Fig. 8). The function $F(E_0, l_c)$ is defined here by the right-hand side of Eq. (29).

III. MODE-LOCKED REGIMES

The theory developed above allows us to calculate all pulse parameters for similariton regimes in the ring laser. These mode-locked regimes are critically dependent on the the laser parameters, which can be found by taking into account the periodic boundary condition for propagating similariton pulses. We may write this periodic boundary condition for input pulses (at $z = 0$) in the first similariton propagation segment as

$$\psi_0(\tau) = K^{1/2}\psi_F(\tau) = K^{1/2}R(E_0, l_c)h(\tau). \tag{36}$$

Because we assume that the threshold of Eq. (31) is satisfied, the periodic boundary condition yields the equation $\tau_0 = \Lambda\tau_{s0}$. Here τ_{s0} is the width of the similariton pulse given by Eq. (4) at $l_s = 0$, τ_0 is the width of the input pulse described by the function $\psi_0(\tau)$, and Λ is some dimensionless factor that is approximately equal to one ($\Lambda \simeq 1$). We have introduced this Λ factor because Eq. (4) holds with high accuracy only asymptotically when the distance l_s is sufficiently long and the pulse is parabolic. From Eq. (33), it follows that $\tau_0 = \tau_h$, and hence the periodic boundary condition for the pulses propagating in the ring laser can be written in the form $\tau_h = \Lambda\tau_{s0}$, or in an explicit form as

$$\tau_h = 3\Lambda\left(\frac{\beta_s\gamma_s E_0}{2g_s^2}\right)^{1/3}. \tag{37}$$

This equation holds in the general case because Eq. (36) yields the condition $\tau_0 = \tau_h$ for an arbitrary filter function $h(\tau)$. Note that we assume the condition $\tau_h \gg \tau_c$, where $\tau_c \geqslant 0.6$ ps for propagation regime described by Eq. (7); hence, we find $\tau_h \gg 0.6$ ps.

Our direct simulations show that if the filter function is Gaussian $H(\omega) = \exp(-\tau_h^2\omega^2/2)$, then the Λ factor can be chosen equal to one. Thus, if the threshold Eq. (31) is satisfied for some parameter $K \leqslant 1$, then the input energy E_0 of the pulse for stable laser regime is

$$E_0 = \frac{2g_s^2\tau_h^3}{27\beta_s\gamma_s}. \tag{38}$$

In the next section we demonstrate that for stable regimes this equation holds with good accuracy. This equation is also satisfied well in the more general case when the filter function has an arbitrary shape.

We also have found that the necessary condition for this scheme of ring laser is $\tau_h \gg \tau_c$, which using Eq. (37) can be written in an explicit form as

$$E_0 \gg 0.7\frac{\sqrt{g_s\beta_s}}{\gamma_s}\exp\left(-\frac{1}{2}g_s l_s\right). \tag{39}$$

From this inequality it follows that for fixed input energy E_0, the length l_s of the first amplifying segment should be enough long to generate the required energy $E_s = E_0 e^{g_s l_s}$ at $z = l_s$ of the parabolic pulse in the first segment. Otherwise, the compression in the second segment is not effective to generate mode-locked operation in the similariton laser.

From this theory it follows that the train of highly linearly chirped output similariton pulses in the ring laser is given by

$$\psi_{\text{out}}(\tau) = \sqrt{1-\kappa_s}\,\hat{\psi}_s(\tau), \tag{40}$$

with

$$\hat{\psi}_s(\tau) = \sum_{N=0}^{\infty}\psi_s\left(E_0^{(N)}, \tau - N\tau_R\right). \tag{41}$$

Here the function $\psi_s(E_0,\tau) = \psi_s(\tau)$ is defined by Eqs. (2)–(5), τ_R is the round-trip time of the pulse in the laser, and the energy $E_0^{(N)}$ is the characteristic input energy of the similariton pulse after N propagating round trips. In the general case, this energy $E_0^{(N)}$ deviates from the input energy $E_0 = E_0^{(0)}$ at $N = 0$.

The generated train of output parabolic pulses also can be compressed by a special fiber with an anomalous GVD and zero nonlinear parameter coupled to the couple κ_s. One can use for such compression the same fiber as for the second compression segment, and at length l_c the output compressed pulses are

$$\begin{aligned}\psi_{\text{out}}^c(\tau) &= \sqrt{1-\kappa_s}\int_{-\infty}^{+\infty}\mathcal{G}(l_c,\tau-\tau')\hat{\psi}_s(\tau')d\tau' \\ &= \sqrt{\kappa_s^{-1}-1}\sum_{N=0}^{\infty}\psi_c\left(E_0^{(N)}, l_c, \tau - N\tau_R\right),\end{aligned} \tag{42}$$

where the function $\psi_c(E_0, l_c, \tau) \equiv \psi_c(l_c, \tau)$ is given by Eq. (15). The compressed periodic output pulses in this case will be Gaussian with a good accuracy. Moreover, it follows

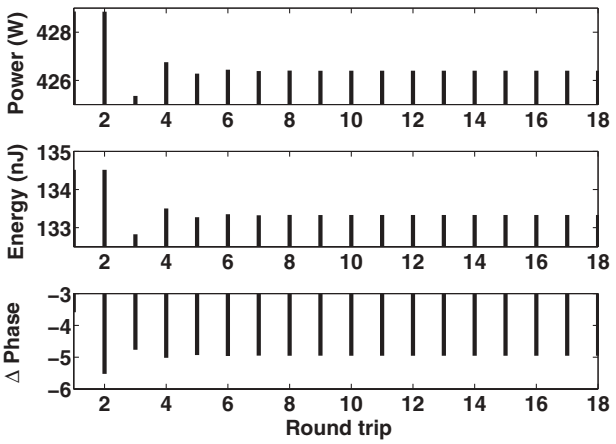

FIG. 2. Peak power, energy, and Δ_{phase} at point A as a function of number N of round trips for the SP1 regime.

from Eq. (42) that the spectrum of the train of output pulses is parabolic and coincides with the spectrum of similariton pulses given by Eq. (41) (see Fig. 6).

We also can define the deviation of the pulse phase $\Delta_{\text{phase}}^{(N)} = \Phi_s^{(N+1)}(0) - \Phi_s^{(N)}(0)$ for the Nth round trip where the phase $\Phi_s^{(N)}(0)$ is defined by Eq. (5); hence, $\Delta_{\text{phase}}^{(N)}$ is

$$\begin{aligned}\Delta_{\text{phase}}^{(N)} &= \left[\Phi_0^{(N+1)} - \Phi_0^{(N)}\right] \\ &\quad + \frac{3\gamma_s}{8g_s}\left(\frac{2g_s^2}{\beta_s\gamma_s}\right)^{1/3}\left\{\left[E_0^{(N+1)}\right]^{2/3} - \left[E_0^{(N)}\right]^{2/3}\right\}.\end{aligned} \tag{43}$$

The deviation of the pulse phase $\Delta_{\text{phase}}^{(N)}$ as the function of the number N has period one for the stable pulse SP1 regime and it has period two for the SP2 regime (see Figs. 2 and 3). For unstable regimes, the function $\Delta_{\text{phase}}^{(N)}$ is aperiodic (see Fig. 4). This behavior of $\Delta_{\text{phase}}^{(N)}$ also can be demonstrated using Eq. (43).

IV. DETERMINATION OF LASER PARAMETERS

Direct numerical simulations of pulse propagation in the ring laser for different laser parameters have demonstrated

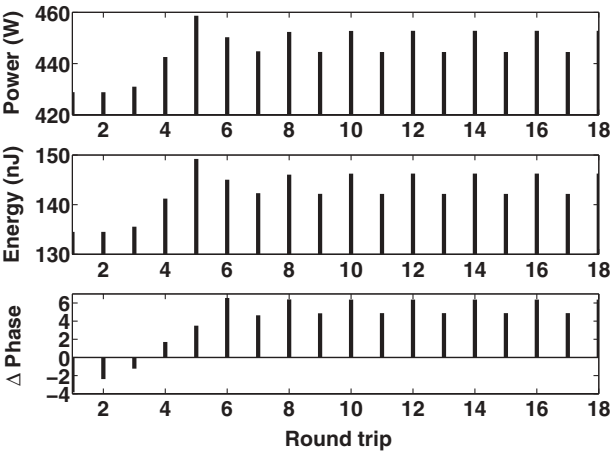

FIG. 3. Peak power, energy, and Δ_{phase} at point A as a function of number N of round trips for the SP2 regime.

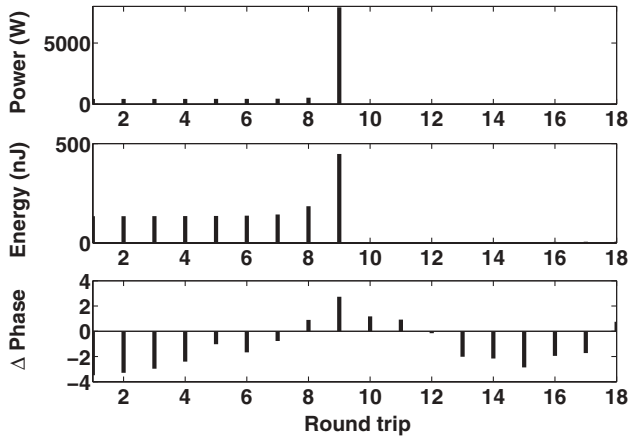

FIG. 4. Peak power, energy, and Δ_{phase} at point A as a function of number N of round trips for the unstable regime.

three basic similariton regimes: SP1 (period of one round trip) (Fig. 2), SP2 (period of two round trips) (Fig. 3), and unstable (Fig. 4). In the results presented later in this article we are mostly interested in the first two similariton propagation regimes. In this section we describe the simulation of the laser and pulse parameters chosen from the developed theory, assuming that the Raman gain g_s and the parameters of the fiber in all segments are fixed. Thus, we should determine the laser parameters such as l_s, κ_s, l_c, κ_0, l_0, τ_h, K, and the characteristic energy E_0 of the similariton pulse given by Eq. (6) for the SP1 or SP2 regime as in Figs. 2 and 3, respectively. The laser and pulse parameters can be found in the following way:

1. First, we fix some available value of the filter width $\tau_h \gg 0.6$ ps and then calculate the energy E_0 by Eq. (38). One also can decide on the energy E_0 that one would like to have at the input of the first amplifying segment. Then the filter width for $\tau_h \gg 0.6$ ps is given by Eq. (37) with $\Lambda = 1$.
2. Using the input function $\psi_0(\tau)$ given by

$$\psi_0(\tau) = \frac{\sqrt{E_0}}{||h||} h(\tau) e^{i\phi_0},$$
$$||h|| \equiv \left[\int_{-\infty}^{+\infty} |h(\tau)|^2 d\tau\right]^{1/2}, \tag{44}$$

[or by Eq. (33) in the case of Gaussian filter function], we choose the length l_s to be such that the pulse function $\psi_s(\tau)$ in the end of the first segment coincides with the function given by asymptotical parabolic solution [Eqs. (2)–(6)]. This can be verified by numerical solution of the GNLSE [Eq. (1)]. Moreover, for a given energy E_0, the length l_s should satisfy the inequality Eq. (39) as well.
3. In this step, we choose the coupling parameter $0 < \kappa_s < 1$ to yield a sufficient amount of the light in the cavity to satisfy the threshold condition Eq. (31) for appropriate attenuator parameter $K \leqslant 1$. Then the output parabolic laser pulse is given by $\psi_{\text{out}}(\tau) = \sqrt{1-\kappa_s}\psi_s(\tau)$ and the energy of the output parabolic pulse is

$$E_{\text{out}} = \int_{-\infty}^{+\infty} |\psi_{\text{out}}(\tau)|^2 d\tau = (1-\kappa_s) E_0 \exp(g_s l_s). \tag{45}$$

4. We calculate the compression length l_c from the condition that the chirp of the pulse in the end of second segment (at $z = l_c$) for $\tau = 0$ is close to zero. Note that for the SP1 and SP2 regimes the chirp is not exactly equal to zero. This compression length l_c can be found approximately as in Eq. (18) or more accurate by Eq. (7). For different values of the parameter l_c close to this, the laser demonstrates three similariton regimes: SP1 (Fig. 2), SP2 (Fig. 3), and unstable (Fig. 4). These regimes can be checked by numerical simulations for large numbers of round trips in the ring laser. The function $\psi_c(\tau)$ in the second compressing segment at $z = l_c$ is given by Eq. (7) and in analytical form by Eq. (15).
5. We choose the coupling parameter κ_0 close to 0.5 ($\kappa_0 \neq 0.5$) to yield sufficient nonlinear feedback. For example, if one fixes the value $\kappa_0 = 0.52$, then the parameters l_0 and L_0 can be found as in Eq. (22). The output filter function $\psi_F(\tau)$ is defined by Eq. (24). Because we assume that $\tau_h \gg \tau_c$, a good approximation is given also in Eq. (26). However, to assess different similariton regimes for large numbers of round trips in the ring laser, Eq. (24) or direct simulations along the Sagnac loop should be used. The reason is that in the approximate solution Eq. (26) the filter function $\psi_F(\tau)$ and hence the function $\psi_0(\tau)$ are unchirped. However, even a small chirp in the pulse $\psi_0(\tau)$ after numerous round trips yields some noise in the laser cavity and leads to different similariton regimes.
6. In this step we calculate the attenuator parameter $K \leqslant 1$, which should satisfy the laser threshold condition Eq. (31) or Eq. (29):

$$K = \frac{E_0}{|R|^2}\left[\int_{-\infty}^{+\infty} |h(\tau)|^2 d\tau\right]^{-1} = \frac{2\pi E_0}{|R|^2}\left[\int_{-\infty}^{+\infty} |H(\omega)|^2 d\omega\right]^{-1}, \tag{46}$$

with the square of the amplitude $|R|^2$ given by

$$|R|^2 = \kappa_0^2 |R_1|^2 - \kappa_0(1-\kappa_0)(R_1 R_2^* + R_2 R_1^*) + (1-\kappa_0)^2 |R_2|^2. \tag{47}$$

In the particular case of a Gaussian filter function, Eq. (46) yields

$$K = 2\sqrt{\pi}\tau_h E_0 |R|^{-2}. \tag{48}$$

Using direct simulation the parameter K can be found by equation $K = E_0/E_{\text{F}}$ where E_{F} is the energy of the pulse in the first round trip propagating between variable attenuator and the FSLD.
7. The SP1 and SP2 regimes exist for a range of laser parameters. If we define the laser parameters as described earlier in this article, one may choose the parameter l_c as a single parameter defining the regions of different

laser regimes. This is because the SP1 and SP2 regimes exist only when the output function $\psi_c(\tau)$ in a second segment (at $z = l_c$) has just a small chirp. Thus, these regimes exist around the value $l_c \simeq 3\beta_s/(g_s|\beta_c|)$. To define the ranges of the parameter l_c for which these similariton regimes exist, we use the direct numerical simulations for propagating pulses around the ring laser with large numbers of round trips $N \gg 1$. These simulations are necessary because the laser regimes are sensitive to any noise background in the fiber ring laser.

V. NUMERICAL SIMULATIONS

The numerical results obtained in this article are based on direct simulation of the GNLSE [Eq. (1)] with appropriate fiber parameters in each section of the ring similariton laser, using well known split-step Fourier method [33] for tens of thousands of round trips N of the propagating field. The filter is simulated in accordance with its definition by Eq. (23) while the response of the attenuator, the coupler, and the isolator are taken into account by integrating their respective loss in the code. In these simulations we assume that the input of the light in each stage is equal to the output of the previous stage. The initial conditions vary from some given pulses to initial noise in the cases when self-starting regimes are expected. We note that even if the initial field does not have a noise component, the simulation for the number of round trips $N \gg 1$ yields small power noise components of the propagating field which are important for reaching different laser regimes (SP1, SR2, or unstable regimes). Thus, all numerical results have been obtained by direct simulations of the GNLSE for the propagating field in each section with the number of round trips $N \gg 1$.

The numerical simulations show (see Fig. 2) that in the SP1 regime the characteristic energy $E_0^{(N)}$ of the similariton pulse after large number N of round trips is the constant $E_0^{(N)} = \bar{E}_0$ for $N \gg 1$, and $\bar{E}_0$ slightly differs from the input energy $E_0 = E_0^{(0)}$ calculated by Eq. (38). In the SP2 regime (see Fig. 3) we have two different energies, $E_0^{(N)} = \bar{E}_0{}'$ and $E_0^{(N)} = \bar{E}_0{}''$ for odd and even N, respectively, when $N \gg 1$. These two values $\bar{E}_0{}'$ and $\bar{E}_0{}''$ are different but also close to the energy E_0 in Eq. (38).

For the numerical simulation, all the parameters of the laser have been set to values typically found in available optical components. The similariton stage should be long enough to support a parabolic pulse which is only reached asymptotically. The first coupler κ_s should be chosen in order to have a reasonable amount of the light in the cavity while maximizing the output power of the laser, while the second coupler κ_0 should be as close to 50/50 as possible to have a good contrast in the SLD. The numerical results presented in this section are found for the case $E_0 = 5$ pJ, $l_s = 1700$ m, $g_s = 0.006$ m^{-1}, $\beta_s = 0.13$ ps^2 m^{-1}, $\gamma_s = 0.002$ W^{-1} m^{-1}, $\beta_c = -0.021$ ps^2 m^{-1}, $\gamma_0 = 0.013$ W^{-1} m^{-1}, $\kappa_s = 0.1$, $\kappa_0 = 0.52$, while the loss of the fibers is set to a typical 0.2 dB/km ($= 4.6 \times 10^{-5}$ m^{-1}) and the length of the SLD is set by Eq. (22). The filter is then chosen to set τ_h to the value given by Eq. (37), which is $\tau_h = 7.87$ ps. The output energy of the pulse after the isolator is then set to E_0 by using a variable attenuator. In the cases given later in this article, l_0 is found to be close to 0.5 m and K is close to 0.5.

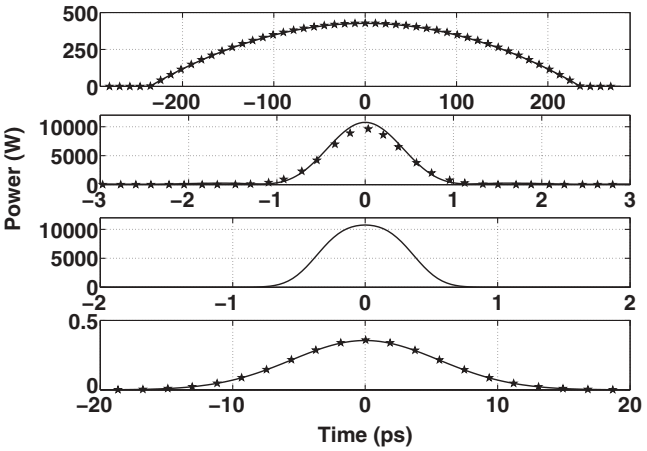

FIG. 5. Pulses at points A, B, C, and D for the SP1 regime. Solid curves represent the numerical simulations and stars represent the analytical solutions: Eq. (2) for A, Eq. (15) for B, and Eq. (33) for D.

As described earlier in this article, we have found three operating regimes for the laser which correspond to three values of the net dispersion of the cavity. These three regimes are implemented in the simulation by varying the length l_c of the fiber used in the linear compression stage around $\tilde{l}_c = 3095$ m, which is the value found from Eq. (18). For these parameters, the SP1 regime exists for a length l_c around $l_c = 3076$ m (which corresponds to $E_0^{(N)} = 4.95$ pJ and the net GVD of the cavity, strongly in the normal regime, is $\beta_{\text{net}} = 156.39$ ps^2), and the SP2 regime exists for $l_c > 3085$ m ($\bar{E}_0{}' = 5.2843$ pJ, $\bar{E}_0{}'' = 5.4366$ pJ, and $\beta_{\text{net}} = 156.19$ ps^2) and unstable regimes exist for length l_c smaller than $l_c < 3072$ m ($\beta_{\text{net}} = 156.49$ ps^2). The peak power of the pulse, the energy, and the phase difference of the pulse between each round trip for the SP1 regime, the SP2 regime, and the unstable regime are shown in Figs. 2, 3, and 4, respectively. In the three cases described here, the cavity has been designed to have an output energy after the first round trip to be equal the input energy $E_0 = 5$ pJ.

In the stable regime, the shape of the pulse varies along the cavity, as shown in Fig. 5. We can verify that the intensity before and after the first segment matches exactly the analytical expression given by Eq. (33) (in D) and Eq. (2) (in A) while the pulse in B is well approximated by the expression given in Eq. (15). The spectrum and the frequency chirp in A, B, C, and D are also shown in Fig. 6 and Fig. 7, respectively. The spectra at points A and B are the same, which follows from Eq. (7). The spectrum at point D is Gaussian and it coincides exactly with spectrum for analytical solution in Eq. (33).

As mentioned earlier in this article, this numerical study concerns a seeded laser even if we expect the laser to be self-starting in some cases or with a slightly different scheme to be described elsewhere. In the cases shown here, the stability of the laser is dependent on the input energy of the seed. The design of the laser is fixed (i.e., l_c, l_0, and K are the value found for the case $E_0 = 5$ pJ) and the output energy $F(E_0, l_c)$

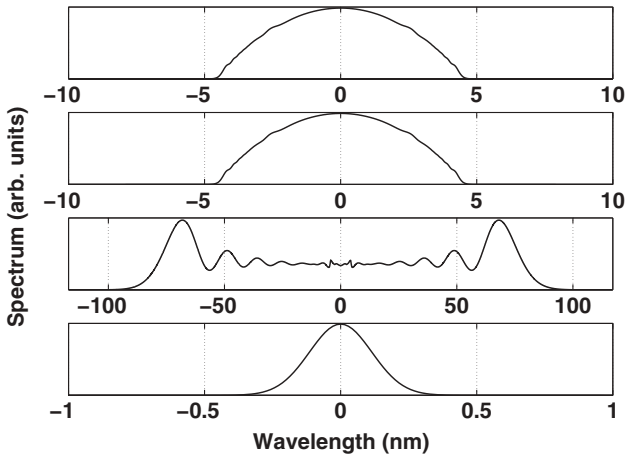

FIG. 6. Spectrum at points A, B, C, and D for the SP1 regime. Solid curves represent the numerical simulations. The spectra at points A and B are parabolic and coincide exactly with theoretical spectrum for the solution in Eq. (2).

can then be numerically calculated as

$$F(E_0, l_c) = K \int_{-\infty}^{+\infty} |\psi_F(\tau)|^2 d\tau. \tag{49}$$

The thick curves in Fig. 8 represent the output energy $F(E_0, l_c)$ after one round trip as a function of the input energy of the seed E_0. Figure 8 shows that the output energy after one round trip is an oscillating function of the input energy E_0. We note that the laser threshold condition Eq. (31) is equivalent to Eq. (29), which we may rewrite now in the form $E_0 = F(E_0, l_c)$. Hence, the points of energy for which the linear curve $f(E_0) = E_0$ (thin curve in Fig. 8) and thick curve $F(E_0, l_c)$ intersect at points where the output energy after one round trip is exactly the same as the input energy. For these points (energies E_0), the laser threshold condition [Eq. (31)] is satisfied.

The dotted square regions in Fig. 8 show the continuous range of input energies leading to the stable SP1 (top panel)

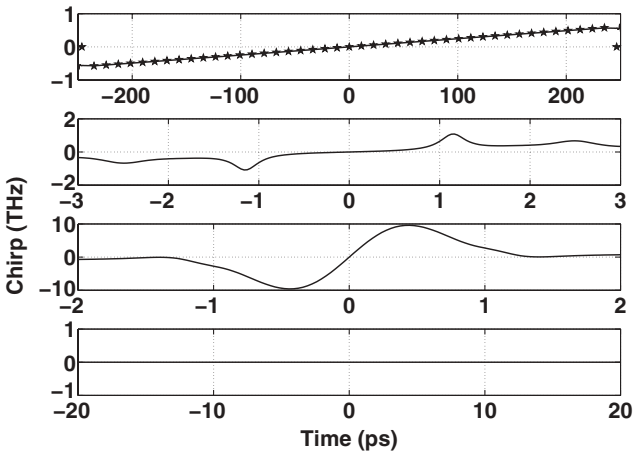

FIG. 7. Frequency chirp at points A, B, C, and D for the SP1 regime. Solid curves represent numerical simulations and stars represent the analytical solution for linear chirp $\Omega_s(\tau) = g_s\tau/(3\beta_s)$ at point A (similariton chirp). Theoretical and numerical chirps at point D are equal to zero.

and SP2 (middle panel) regimes presented earlier in this article. For the SP1 regime, the input energy E_b represents the maximum energy allowed to get a stable regime. If the input energy is greater than E_b, the output energy after the first round trip will be greater than the input energy and will keep increasing, which leads to a nonstable regime. Graphically, E_b corresponds to the last intersection point between the thin curve and the thick curve. For input energies smaller than E_a, output energies after the first round trip could also be greater than E_b or smaller than E_a, also leading to unstable regimes. However, stable regimes could also be found for specific input energies smaller than E_a, leading to an output energy in the range $[E_a, E_b]$ after several round trips. As mentioned earlier in this article, the stabilized energy for the SP1 regime is $E_0^{(N)} = 4.95$ pJ and it is not dependent on the input energy.

Following the same reasoning for the SP2 regime, the maximum energy corresponds to E_d, while the minimum energy E_c is $E_0 = 5$ pJ in the dotted square region in Fig. 8. For some input energies smaller than E_0, the output energies could decrease rapidly and become smaller than the smallest input energy allowed by the threshold condition. We do not present here the detail graphs for SP2 regimes (see Fig. 3) because they have the same pulse shape as for SP1 regimes. Furthermore, numerically, SP2 regimes start up for small changes of laser parameters (here we vary the length l_c) but it is difficult to distinguish SP1 from SP2 using analytical curves because they are approximate, as expected. The numerical simulation also shows only small deviations in the parameters of two sequential pulses in SR2 regimes. The shapes of such sequential pulses are exactly the same as in SP1 regimes and they are determined by their sequential energies, which are $\bar{E}_0{}' = 5.2843$ pJ and $\bar{E}_0{}'' = 5.4366$ pJ when $l_c >$ 3085 m (Fig. 3). The theory for the SP1 regime [see Eq. (38)] yields the energy $E_0 = 5$ pJ; hence, in this case the fractional deviation of the numerical result from the analytic result is $|\bar{E}_0 - E_0|/E_0 = 1\%$. The deviations of energies for the SP2 regime are $|\bar{E}_0{}' - E_0|/E_0 \simeq 6\%$ and $|\bar{E}_0{}'' - E_0|/E_0 \simeq 9\%$, respectively, which demonstrates that, in the case of the SP2 regime, Eq. (38) gives less accuracy. For the unstable regime (shown in the bottom panel of Fig. 8), only one intersection point exists between the thin line and the thick line, resulting in the energy rapidly increasing as soon the input energy deviates slightly from E_0. Hence, this case leads to unstable operation and decreasing power of the pulses to zero for large number of the round trips.

The analysis in this section is based on direct simulation of the GNLSE in each section of the ring laser with tens of thousands of round trips N. The output energy $F(E_0, l_c)$ in Eq. (49) is also found by numerical simulation. However, the output energy $E_0 = F(E_0, l_c)$ can be calculated with a good accuracy analytically [see Eq. (29)]:

$$F(E_0, l_c) = K|R(E_0, l_c)|^2||h||^2, \quad ||h||^2 = \int_{-\infty}^{+\infty} |h(\tau)|^2 d\tau. \tag{50}$$

This allows us to analyze different regimes using the analytical theory developed earlier. We note here that the presence of small power noise satellite components of the light is also important for reaching different laser regimes and can be taken

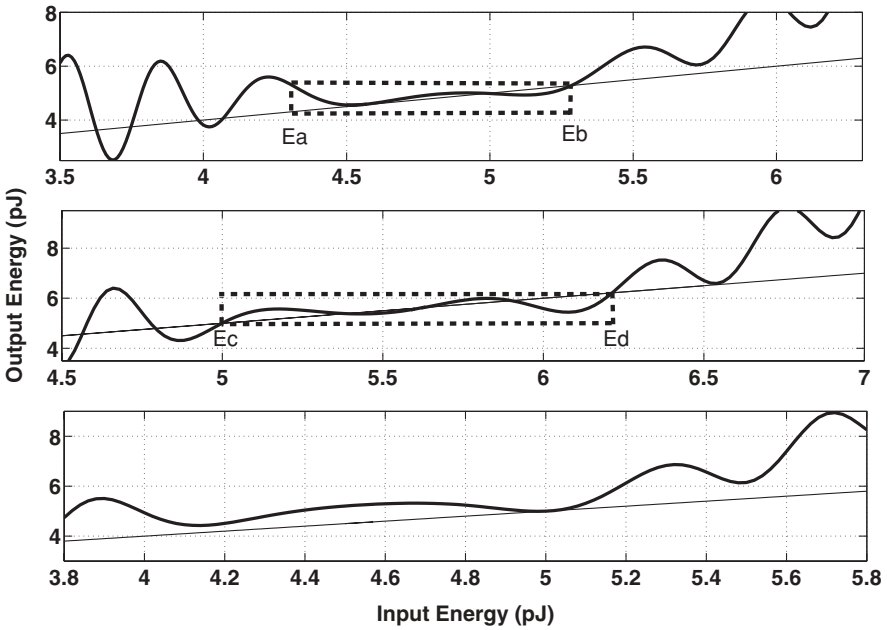

FIG. 8. The thick solid curves represent simulated output energy $F = F(E_0, l_c)$ after the first round trip as a function of input energy E_0 for SP1, SP2, and unstable regimes (top to bottom panels, respectively). The thin solid curves represent the linear function $f(E_0) = E_0$. The dotted squares delineate the largest continuous regions $[E_a, E_b]$ and $[E_c, E_d]$ of E_0 which lead to stable operation (some other isolated starting regions or points outside this region can also lead to stable operation).

into account by direct simulation of the GNLSE discussed earlier in this article.

VI. CONCLUSIONS

We have presented an all-fiber mode-locked similariton laser scheme with Raman amplification designed with the aid of a full theoretical model of its operation. The evolution of a pulse throughout the cavity has been studied theoretically and numerically for various regimes of the laser corresponding to different values of dispersion of the cavity. The output similariton pulses of the laser have a true parabolic shape and a linear chirp, and stable pulses can exist with the much greater energies that can be achieved in solitonlike laser. Previously developed similariton lasers [19–25] have all been based on high-gain, rare-earth doped fiber sections, which limits their operation to the gain regions of these amplifiers. In addition, these laser designs generally rely upon free space elements which are less practical than the all-fiber system proposed here. Since the gain is achieved by Raman amplification, this laser could operate in a broad range of wavelengths. External compression of the parabolic similaritons can be used to achieve high peak power pulses, and the all-fiber nature of the laser lends itself to a compact stable implementation which could find application in a range of devices. The design proposed here utilizes a mode-locking mechanism and the system should be readily adaptable to operate over a wide range limited primarily by the availability of suitable pump lasers and filters.

APPENDIX: GAUSSIAN APPROXIMATION

In this appendix we calculate the function $\psi_c(z, \tau)$ in the second compression segment. This function for $z = l_c$ is given by Eq. (7) with the Green function defined in Eq. (8). Because it is impossible to calculate the integral in Eq. (7) analytically, we develop here an approximate method. The treatment is based on an assumption that for some length l_c the function $\psi_c(z, \tau)$ can be described with a good accuracy with a Gausssian function in the case when $\beta_c < 0$. This conjecture has been confirmed by numerous simulations for specific length $z = l_c$ for which the chirp of the propagating pulse is close to zero. Thus, l_c is the length for which the chirp of the parabolic pulse is compensated by linear compression. Because a linearly chirped Gaussian pulse in a linear dispersive medium maintains its Gaussian shape on propagation, we approximate in our calculations (for some length l_c discussed above) the input parabolic pulse $\tilde{\psi}_s(\tau) = \kappa_s^{1/2}\psi_s(\tau)$ in Eq. (7) with a linearly chirped Gaussian pulse having the same energy, effective width, and chirp. Thus, the input pulse in the second compression segment given by

$$\tilde{\psi}_s(\tau) = \tilde{A}_s\sqrt{1-\left(\frac{\tau}{\tau_s}\right)^2}\exp[i\Phi_s(\tau)]\theta(\tau_s - |\tau|), \quad \text{(A1)}$$

$$\tilde{A}_s = \sqrt{\kappa_s}A_s = \frac{\sqrt{\kappa_s}}{2}\left(\frac{2g_s^2E_0^2}{\beta_s\gamma_s}\right)^{1/6}\exp\left(\frac{1}{3}g_sl_s\right) \quad \text{(A2)}$$

in this approximation can be replaced with the linearly chirped Gaussian pulse as

$$\psi_g(\tau) = A_g\exp\left(-\frac{\tau^2}{2\tau_g^2} - \frac{i}{2}C\tau^2 + ia\right). \quad \text{(A3)}$$

We choose here the same phase parameters of the Gaussian pulse as in the input parabolic pulse: $a = \Phi_0 + 3\gamma_sA_s^2/2g_s$ and $C = g_s/3\beta_s$. To find unknown parameters τ_g and A_g, we assume that the energies and the effective widths of the input pulses $\tilde{\psi}_s(\tau)$ and $\psi_g(\tau)$ are also the same:

$$\int_{-\infty}^{+\infty}|\tilde{\psi}_s(\tau)|^2d\tau = \int_{-\infty}^{+\infty}|\psi_g(\tau)|^2d\tau, \quad \text{(A4)}$$

$$\int_{0}^{+\infty}|\tilde{\psi}_s(\tau)|^2\tau d\tau = \int_{0}^{+\infty}|\psi_g(\tau)|^2\tau d\tau. \quad \text{(A5)}$$

These equations with wave functions given by Eqs. (A1) and (A3) yield the relations

$$\frac{4}{3}\tilde{A}_s^2\tau_s = \sqrt{\pi}A_g^2\tau_g, \quad \frac{1}{4}\tilde{A}_s^2\tau_s^2 = \frac{1}{2}A_g^2\tau_g^2, \tag{A6}$$

which define the parameters τ_g and A_g of the Gaussian pulse in explicit form as

$$\tau_g = \frac{3\sqrt{\pi}}{8}\tau_s, \quad A_g = \frac{4}{3}\sqrt{\frac{2}{\pi}}\tilde{A}_s. \tag{A7}$$

Using in Eq. (7) the function $\psi_g(\tau)$ instead of $\tilde{\psi}_s(\tau)$, one may calculate the integral in explicit form. Another equivalent approach is based on the Fourier method [33]. In this method, we introduce the Fourier transform of the $\psi_g(\tau)$: $\Psi_g(\omega) = \int_{-\infty}^{+\infty}\psi_g(\tau)e^{i\omega\tau}d\tau$, which is

$$\Psi_g(\omega) = \tau_g A_g\sqrt{\frac{2\pi(1-iG)}{1+G^2}}\exp\left[-\frac{\tau_g^2(1-iG)}{2(1+G^2)}\omega^2\right]e^{ia}, \tag{A8}$$

where $G = C\tau_g^2$ is the dimensionless parameter. The propagation of the Gaussian pulse in a linear dispersive medium ($\beta_c < 0$) is described by equation

$$\psi_c(z,\tau) = \frac{e^{-\alpha_c z/2}}{2\pi}\int_{-\infty}^{+\infty}\Psi_g(\omega)\exp\left(\frac{i}{2}\beta_c\omega^2 z - i\omega\tau\right)d\omega. \tag{A9}$$

The integration in Eq. (A9) yields the function $\psi_c(z,\tau)$ as

$$\psi_c(z,\tau) = \frac{\tau_g A_g e^{-\alpha_c z/2}}{\sqrt{\tau_g^2 + \beta_c G z - i\beta_c z}} \times \exp\left[-\frac{\tau^2}{2T(z)^2} - \frac{i}{2}C(z)\tau^2\right]e^{ia}, \tag{A10}$$

where the width $T(z)$ and the phase function $C(z)$ are

$$T(z) = \tau_g\sqrt{1 + \frac{2\beta_c G}{\tau_g^2}z + \frac{\beta_c^2}{\tau_g^4}(1+G^2)z^2}, \tag{A11}$$

$$C(z) = \frac{G\tau_g^2 + (1+G^2)\beta_c z}{\tau_g^4 + 2\tau_g^2\beta_c G z + (1+G^2)\beta_c^2 z^2} = \frac{G\tau_g^2 + (1+G^2)\beta_c z}{\tau_g^2 T(z)^2}. \tag{A12}$$

If we define the characteristic length $\tilde{l}_c$ with the equation $C(\tilde{l}_c) = 0$, then we have

$$\tilde{l}_c = \frac{G\tau_g^2}{|\beta_c|(1+G^2)}, \quad G = \frac{g_s\tau_g^2}{3\beta_s}. \tag{A13}$$

Combining Eqs. (A11) and (A13), we find an important relation:

$$\left[\frac{d}{dz}T(z)\right]_{z=\tilde{l}_c} = 0. \tag{A14}$$

Using Eq. (A14) we may rewrite the function given by Eq. (A10) in the vicinity of $z = \tilde{l}_c$ as

$$\psi_c(z,\tau) = \mathcal{A}\exp\left[-\frac{\tau^2}{2\tau_c^2} - \frac{\alpha_c z}{2} - \frac{i}{2}\mathcal{C}(z)\tau^2\right]e^{ia}, \tag{A15}$$

where the phase function $\mathcal{C}(z)$ and the amplitude $\mathcal{A}$ are

$$\mathcal{C}(z) = \frac{G}{\tau_c^2} - \frac{|\beta_c|}{\tau_c^4}z, \tag{A16}$$

$$\mathcal{A} = A_g\sqrt{1-iG} = \frac{4}{3}\sqrt{\frac{2\kappa_s}{\pi}}(1+G^2)^{1/4}A_s e^{i\Phi/2}. \tag{A17}$$

Here $\Phi = \arctan(-G)$, and the parameters G, τ_c, and $\tilde{l}_c$ are given by

$$G = \frac{g_s\tau_g^2}{3\beta_s} = \frac{3\pi g_s\tau_s^2}{64\beta_s}, \tag{A18}$$

$$\tau_c = \frac{\tau_g}{\sqrt{1+G^2}} = \frac{3\sqrt{\pi}\tau_s}{8\sqrt{1+G^2}}, \tag{A19}$$

$$\tilde{l}_c = \frac{G\tau_g^2}{|\beta_c|(1+G^2)} = \frac{G\tau_c^2}{|\beta_c|}. \tag{A20}$$

We have neglected the nonlinear effects in the compression segment; hence, the next condition should be fulfilled in the compression segment:

$$\frac{L_D}{L_{NL}} = \frac{\gamma_c\kappa_s A_s^2\tau_c^2}{|\beta_c|} \ll 1, \tag{A21}$$

where L_D and L_{NL} are the dispersion length and nonlinear length, respectively. In conclusion, we emphasize that the results obtained in this appendix are correct only for distances $|z-\tilde{l}_c|/\tilde{l}_c \ll 1$, where the characteristic length $\tilde{l}_c$ is defined by condition $\Omega_c(z,\tau)|_{z=\tilde{l}_c} = \mathcal{C}(\tilde{l}_c)\tau = 0$ [where $\Omega_c(z,\tau)$ is the chirp of the pulse]. The equations obtained here are in a good agreement with numerical simulations (see Fig. 5). In particular, Eq. (A20) for characteristic length $\tilde{l}_c$ gives the deviation from numerical results as about 1%.

[1] O. E. Martinez, R. L. Fork, and J. P. Gordon, Opt. Lett. **9**, 156 (1984).

[2] H. A. Haus, J. G. Fujimoto, and E. P. Ippen, IEEE J. Quantum Electron. **28**, 2086 (1992).

[3] K. Tamura, J. Jacobson, H. A. Haus, E. P. Ippen, and J. G. Fujimoto, Opt. Lett. **18**, 1080 (1993).

[4] B. Proctor, E. Westwig, and F. Wise, Opt. Lett. **18**, 1654 (1993).

[5] H. A. Haus, J. G. Fujimoto, and E. P. Ippen, J. Opt. Soc. Am. B **8**, 2068 (1991).

[6] M. E. Fermann, V. I. Kruglov, B. C. Thomsen, J. M. Dudley, and J. D. Harvey, Phys. Rev. Lett. **84**, 6010 (2000).

[7] V. I. Kruglov, A. C. Peacock, J. M. Dudley, and J. D. Harvey, Opt. Lett. **25**, 1753 (2000).

[8] V. I. Kruglov, A. C. Peacock, J. D. Harvey, and J. M. Dudley, J. Opt. Soc. Am. B **19**, 461 (2002).

[9] V. I. Kruglov and J. D. Harvey, J. Opt. Soc. Am. B **23**, 2541 (2006).

[10] C. Finot, G. Millot, C. Billet, and J. Dudley, Opt. Express **11**, 1547 (2003).

[11] C. Finot, S. Pitois, G. Millot, C. Billet, and J. M. Dudley, IEEE J. Sel. Top. Quantum Electron. **10**, 1211 (2004).
[12] C. Finot, G. Millot, and J. M. Dudley, Opt. Lett. **29**, 2533 (2004).
[13] C. Billet, J. Dudley, N. Joly, and J. Knight, Opt. Express **13**, 3236 (2005).
[14] C. Finot, F. Parmigiani, P. Petropoulos, and D. Richardson, Opt. Express **14**, 3161 (2006).
[15] J. Limpert, T. Schreiber, T. Clausnitzer, K. Zöllner, H. Fuchs, E. Kley, H. Zellmer, and A. Tünnermann, Opt. Express **10**, 628 (2002).
[16] A. Malinowski, A. Piper, J. H. Price, K. Furusawa, Y. Jeong, J. Nilsson, and D. J. Richardson, Opt. Lett. **29**, 2073 (2004).
[17] P. D. Drummond and K. V. Kheruntsyan, Phys. Rev. A **63**, 013605 (2000).
[18] V. I. Kruglov, M. K. Olsen, and M. J. Collett, Phys. Rev. A **72**, 033604 (2005).
[19] F. Ö. Ilday, J. R. Buckley, W. G. Clark, and F. W. Wise, Phys. Rev. Lett. **92**, 213902 (2004).
[20] A. Fernandez, T. Fuji, A. Poppe, A. Fürbach, F. Krausz, and A. Apolonski, Opt. Lett. **29**, 1366 (2004).
[21] A. Chong, W. H. Renninger, and F. W. Wise, J. Opt. Soc. Am. B **25**, 140 (2008).
[22] A. Chong, J. Buckley, W. H. Renninger, and F. Wise, Opt. Express **14**, 10095 (2006).
[23] V. L. Kalashnikov, E. Podivilov, A. Chernykh, and A. Apolonski, Appl. Phys. B **83**, 503 (2006).
[24] A. Fernandez, A. Verhoef, V. Pervak, G. Lermann, F. Krausz, and A. Apolonski, Appl. Phys. B **87**, 395 (2007).
[25] J. R. Buckley, F. Ö. Ilday, T. Sosnowski, and F. W. Wise, Opt. Lett. **30**, 1888 (2005).
[26] A. I. Chernykh and S. K. Turitsyn, Opt. Lett. **20**, 398 (1995).
[27] J. Herrmann, V. P. Kalosha, and M. Müller, Opt. Lett. **22**, 236 (1997).
[28] K. M. Spaulding, D. H. Yong, A. D. Kim, and J. N. Kutz, J. Opt. Soc. Am. B **19**, 1045 (2002).
[29] J. M. Soto-Crespo, M. Grapinet, P. Grelu, and N. Akhmediev, Phys. Rev. E **70**, 066612 (2004).
[30] G. E. Falkovich, I. Kolokolov, V. Lebedev, and S. K. Turitsyn, Phys. Rev. E **63**, 025601(R) (2001).
[31] G. Falkovich, I. Kolokolov, V. Lebedev, V. Mezentsev, and S. Turitsyn, Physica D **195**, 1 (2004).
[32] A. Peleg, Phys. Lett. **A373**, 2734 (2009).
[33] Govind P. Agrawal, *Nonlinear Fibre Optics* (Academic Press, San Diego, CA, 2001).